Experimental Research of X-Band Dual-Frequency Coaxial Relativistic Backward Wave Oscillator

HAILONG LI [1] **(Member, IEEE), YIZHENG ZHU** [1], **YONGFU TANG** [2], **LIN MENG** [1] **(Member, IEEE),**
BIN WANG [1] **(Member, IEEE), YONG YIN** [1] **(Member, IEEE), AND MAOYAN WANG** [3]

1 Vacuum Electronic National Laboratory, School of Electronic Science and Engineering, University of Electronic Science and Technology of China, Chengdu 610054, China
2 No. 38 Research Institute, Chinese Electronics Technology Group Corporation, Hefei 230088, China
3 School of Physics, University of Electronic Science and Technology of China, Chengdu 610054, China

CORRESPONDING AUTHOR: H. LI (e-mail: lihailong@uestc.edu.cn)

ABSTRACT The design and experimental demonstration of an X-band coaxial dual-frequency relativistic backward wave oscillator (CRBWO) with sectioned slow wave structures (SWSs) is presented. In this paper, we describe the experimental measurement methods of frequency, power and operation mode for the high-power microwave signal. In experimental tests, with a 500 kV, 11.5 kA beam guided by a 0.82 T magnetic field, a microwave with an average power of 507 MW and pulsewidth of 50 ns has been obtained. Also, the dominant frequencies of the X-band dual frequency are 9.845 GHz and 10.517 GHz, and the dual-frequency difference $\Delta f \approx 672$ MHz, which was similar to the particle-in-cell simulation results. The operation mode of the device is determined to be TM_{01} mode in our experiment.

INDEX TERMS Dual-band, coaxial relativistic backward wave oscillator, sectioned slow-wave structures.

I. INTRODUCTION

High power vacuum electron devices attract many researchers because it is widely used in the industry and in science [1]–[5]. In recent years, more and more researchers have been devoted to the study of HPM pulses with dual frequencies, which has a great application prospect in next generation of war namely electronic warfare (EW) and various communication systems [6]–[8]. This is because dual-frequency HPM has the following advantages. First, microwaves with different frequencies can be generated simultaneously at one burst, which is a huge improvement compared to traditional single-frequency HPMs. Second, only one wideband antenna is needed as the radiation system, so the whole system will be more compact [9].

To produce dual-frequency microwaves, many different dual-frequency devices have been elaborated, including the magnetically insulated line oscillator (MILO) and the relativistic backward wave oscillator (RBWO) [10]–[12]. Ginzburg *et al.* [13] investigated dual-frequency RBWO with

sectioned slow wave structures (SWSs) based on a single relativistic electron-beam. By changing the interaction length of each section of the RBWO, different microwave generation systems can be obtained, i.e., stationary single-frequency, periodic automodulation, and stochastic automodulation regimes. Chen *et al.* [14] designed MILO, which divide a single device into two azimuthal partitions and let each partition have a corresponding resonant frequency, achieving dual-frequency output of S-band and L-band with beam interaction efficiency of 6.5% and 11.0%, respectively. Tang *et al.* [15] have demonstrated an X-band dual-frequency coaxial relativistic backward wave oscillator (CRBWO) with sectioned SWSs and the frequencies of the two dominant frequencies were observed to be 10.06 and 10.49 GHz, respectively. Compared with MILO and other HPM devices, the RBWO has good adaptation to variable electron beam parameters [16]. Teng *et al.* [6] designed a CRBWO with the experimental output frequency and power are 7.40 GHz and 710 MW, respectively.

TABLE 1. Structural parameters.

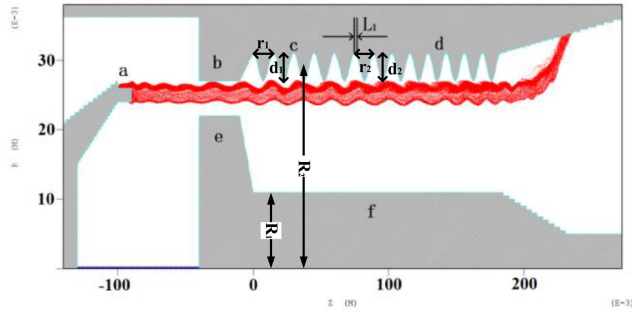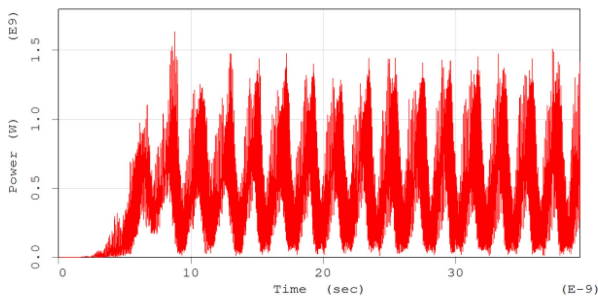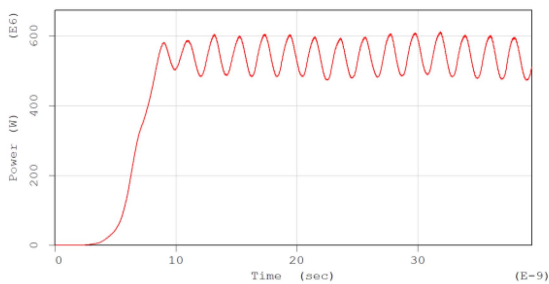| R₁	L₁	R₂	SWS-1			SWS-2		
			r₁	d₁	N₁	r₂	d₂	N₂
11	0.54	29	15	2	5	13.4	2	8

All values are in millimeter.

FIGURE 1. Schematic configuration of the dual-frequency sectioned CRBWO. (a) Annular cathode. (b)Anode. (c) SWSs of the first section. (d) SWSs of the second section. (e) Cut-off neck section. (f) Coaxial smooth waveguide.

(a)

(b)

FIGURE 2. Time development of the PIC simulation results of the dual-frequency CRBWO. (a) Instant microwave power. (b) Average power at the output window.

Wang *et al.* [8] experimentally investigated a dual-band dual annular beams RBWO with dual annular beams, with the powers of the C-band and X-band microwaves of 520 and 113 MW, respectively, and dominant frequencies of 4.58 and 8.30 GHz.

In this paper, based on the research of Tang *et al.* [15], we proposed a CRBWO, which can realize dual-frequency output of single particle beam in X-band, and experimented with this device. It is arranged as follows. In the next section,
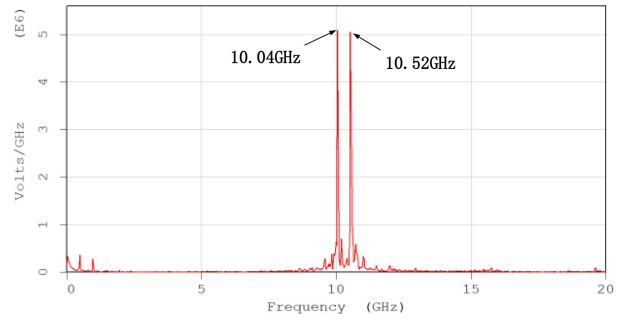

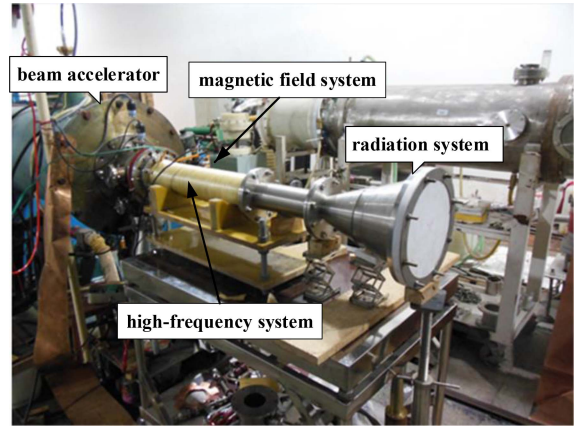**FIGURE 3. Spectrum of dual-band RBWO.**

FIGURE 4. Experimental setup.

we describe the results of particle-in-cell (PIC) simulation of dual-frequency structure. Section III gives the experimental result, and conclusions are stated in Section IV.

II. SIMULATION

The schematic configuration of the X-band dual-frequency sectioned CRBWO is presented in Fig. 1, and its beam-wave regions adopt sectioned SWSs. The SWSs are axisymmetric system whose radius is described by

$$R_{w(z)} = R + \frac{d}{2} * sin(kz) \tag{1}$$

where, z is the axial coordinates, R and d are the mean diameter and depth of corrugation, respectively, $k = 2\pi/r$, and r is axial period of corrugations. The dimensions of the SWSs are summarized in Table 1. Moreover, a smooth drift section of length L_1 is added between the first SWSs and the second SWSs. By changing the length of the drift section, the phase difference between the back wave and the forward wave inside the device can be adjusted.

Before the experiment, to verify the performance of the dual-frequency CRBWO, we performed computer simulations using the 2.5-D particle-in-cell (PIC) code CHIPIC. The annular electron beam emitted the accelerating voltage of 510 kV, and the electron beam current of 8.7 kA. And this beam interacts with the microwaves in SWSs under

the guiding magnetic field of 0.815 T. We can see that the initial oscillation time of the device is 3 ns, and the saturation time is 8 ns in Fig. 2. The peak value of the radiation microwave power of the beat wave is 1.6 GW (Fig. 2(a)). By low-pass filtering of the instant power, we can observe that the average power is $\sim$ 535 MW (Fig. 2(b)).

The fast Fourier transform (FFT) is performed on the electric field signal, as shown in Fig. 3, to obtain the spectrum diagram of the output of the dual-frequency CRBWO. It can be seen that the device realized the dual-frequency output of the x-band, with the dual- frequency of 10.04 GHz and 10.52 GHz, respectively, and the difference of frequency of 0.48 GHz.

III. EXPERIMENT AND RESULTS
A. EXPERIMENTAL SETUP
The experimental system mainly consists of the following parts: (1) Pulsed intense current relativistic electron beam accelerator; (2) Dual-frequency CRBWO high-frequency system; (3) Pulse magnetic field system; (4) Radiation system. The photographs of the accelerator and dual-frequency CRBWO used in the experiment are shown in Fig. 4. The pulsed electron beam accelerator provides a high-powered pulsed electron beam source for the experimental device, which is consists of an ignition control system, a Marx generator, a Blumlein forming line, a main switch, and a vacuum diode. The high voltage pulse generated by the accelerator is applied to the diode, which then emits a relativistic intense current beam with a voltage range of 0.3–1 MV, a current range of 5–10 kA, and a pulse width of about 70 ns.

In the experiment, the accelerator voltage was adjusted at 500 ± 3% kV, which was similar to the PIC simulation results. When the electron beam passed through the SWSs, it generated X-band dual-frequency microwave of the TM_{01} mode. At this time, the device works stably and the guiding magnetic field was 0.82T. In the following experiments, we proposed methods to measure some microwave signal parameters, including frequency, operation mode, and power.

B. FREQUENCY MEASUREMENT
A schematic of the experimental frequency measurement setup is shown in Fig. 5. The microwave signal was received by the far-field horn antenna, and attenuated to the mixer by the coaxial attenuator [17]. At the same time, we input the X-band local oscillator frequency in the mixer. The intermediate frequency signal produced by mixer was filtered by low pass filter and output to digital oscilloscope for measurement. The spectrums of output microwave from several different experiments are shown in Fig. 6. Obviously, the spectrum is pure, the amplitude of dual-frequency component is close, and the width of microwave pulse is $\sim$ 50 ns. It can be obtained that the dual-frequency signal produced by the system is 9.845 ± 2.4% GHz and 10.517 ± 2.1% GHz and dual-frequency difference 672 ± 25.6% MHz.
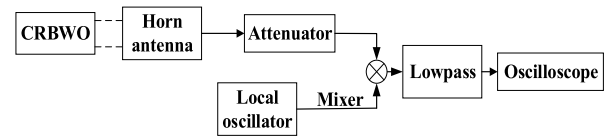

FIGURE 5. Schematic of measurement system with mixing frequency method.

C. MODE MEASUREMENT
The microwave mode measurement adopts the far-field method, and the receiving horn is placed in the far-field of microwave radiation (Fig. 7). It is well known that far-field distance is given by:

$$L > \frac{2D^2}{\lambda} \tag{2}$$

where L is the distance between the horn and the microwave radiation port, D is the maximum size of microwave radiation port surface, and λ is the wavelength of microwave radiation.

During the measurement, one receiving horn antenna was fixed on the maximum radiation direction of the main lobe of the microwave radiation, and the other receiving horn antenna was placed on different receiving direction angles for multiple experiments. Then, the microwave power P_m received by the mobile horn in each experiment and the power P_f received by the fixed horn was normalized, so that the normalized power density spatial distribution of the output microwave radiation can be obtained. As shown in Fig. 8, it can be seen that the experimental measurement results are consistent with the theoretical calculation results, and the microwave radiation mode can be determined as mode TM_{01}.

To verify the correctness of the results, we measured the radiation pattern of microwaves by using a fluorescent lamp array target. The target of fluorescent lamp (Fig. 9 (a)) with an array of 31*31 was placed about 60cm away from the microwave radiation horn, with the center of the target plate and the center of horn antenna at the same level. In the experiment, the strong electric field of microwave ionized the noble gas in the neon lamp of the target plate and generated glow discharge. The luminescence of neon array target was detected by a high-speed camera in the laboratory, and the real-time image was transmitted to the monitor in the experimental control room to display and record synchronously. The measurement results of the fluorescent lamp target are shown in Fig. 9 (b). It can be seen that the shape of the luminescence is annular, and conforms to the characteristics of the TM_{01} mode, which further verifies the correctness of the far-field measurement results.

D. POWER MEASUREMENT
Microwave power is measured by the far-field method, similarly, and the X-band standard rectangular waveguide BJ-100 as the receiver horn. In the experiment, the receiving waveguide is placed at the maximum radiation direction angle of the microwave. After the signal passes through the
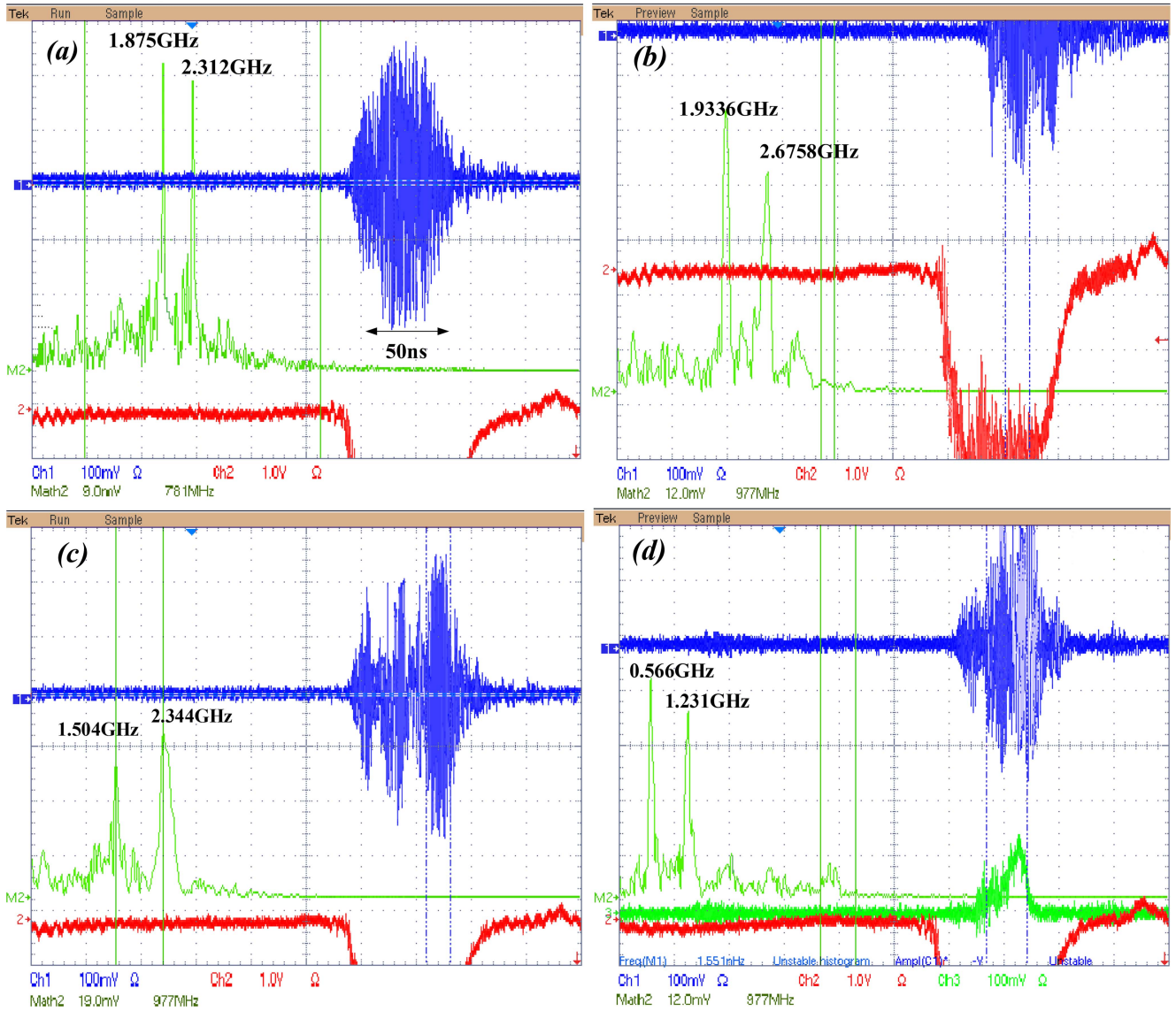
FIGURE 6. The spectrum of output microwave. (a) (b) (c) The spectrum of output microwave from several different experiments when the local oscillator frequency is 8.0 GHz. (d) The spectrum of output microwave when the local oscillator frequency is 9.5 GHz.
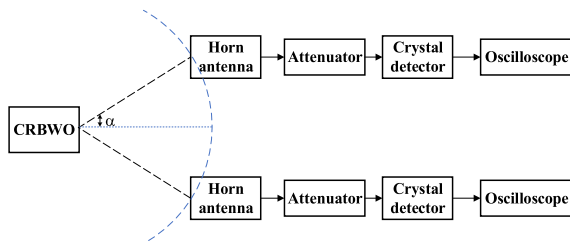

FIGURE 7. Schematic of the far-field method measurement system.

FIGURE 8. Normalized microwave power mode diagram.

waveguide-coaxial converter, coaxial attenuator and crystal detector, the microwave signal is transmitted to the digital oscilloscope. According to the detection signal amplitude obtained by the oscilloscope, the microwave power P_w received by the waveguide can be represented as follows:
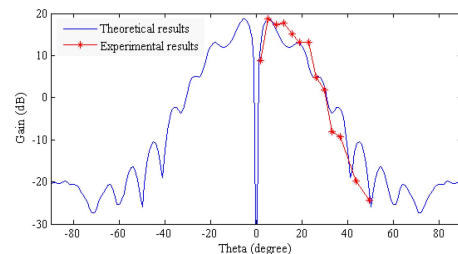
$$P_w = 10^{(V \cdot \xi / K + A)/10} \qquad (3)$$

where ξ is the attenuation coefficient of a signal transmitted to a digital oscilloscope via coaxial line ($\xi \geq 1$), K is the sensitivity of the detection crystal, and A is the attenuation of the microwave attenuator before the detection crystal.

Then, by substituting the expressions (3) into the formula of far-field microwave power measurement
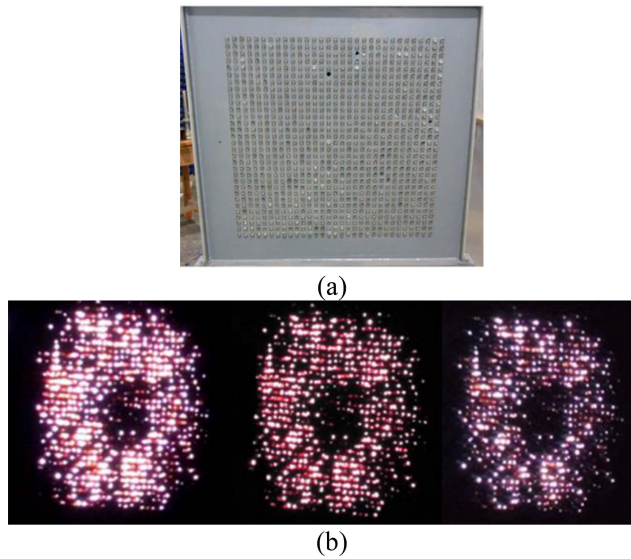
(a)

(b)

FIGURE 9. The microwave mode is measured by fluorescent lamp array target board. (a) Fluorescent lamp target. (b) Measurement results of fluorescent lamp target.
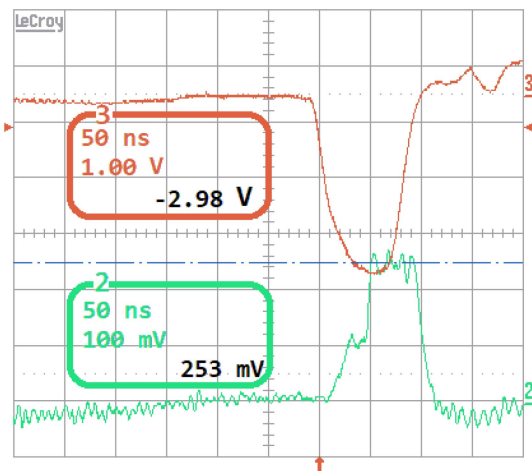

FIGURE 10. Typical microwave power.

formula we obtain:

$$P_s = \frac{4\pi L^2}{D_E} \frac{P_w}{S_{eff}} \tag{4}$$

where, P_s is total power of microwave source, S_{eff} is the effective area of the standard rectangular waveguide at the experimental frequency, and D_E is the directional coefficient of horn antenna of microwave source.

After building the experimental setup, the remaining task is to calibrate the attenuation coefficient ξ, the sensitivity K, and the attenuation A in the experimental frequency (9.8–10.8 GHz). This calibration step is necessary to account for errors due to the approximations used in calculations and tolerances in manufacturing. Moreover, the directional coefficient D_E and the effective area S_{eff} should be calibrated within the experimental frequency range (9.8–10.8 GHz).

The directional coefficient D_E can be represented as follows:

$$D_E = \frac{2}{\int_0^\pi \left(\frac{p_h(\theta)}{p_{hm}} \right) sin(\theta)d\theta} \tag{5}$$

Where, $p_h(\theta)$ is the microwave power measured in any θ direction, and p_{hm} is the microwave power measured in the maximum radiation direction of the microwave radiation horn. The effective area S_{eff} can be represented as follows:

$$S_{eff} = \frac{\lambda^2}{4\pi} D \tag{6}$$

Where, λ is the microwave wavelength, and D is the maximum directivity coefficient of the waveguide. Through calculation, the errors in measuring the effective antenna surface and in calibrating the detector were $\pm 10\%$ and $\pm 5\%$, respectively.

The experiment used pulse accelerator to provide the intense relativistic electron beam with a voltage of $500 \pm 3.0\%$ kV and a current of $11.5 \pm 1.4\%$ kA. This beam interacts with the RF wave in SWSs under behind magnetic field of 0.82 T. The typical waveforms of microwave power measured are shown in Fig. 10 in the experiment. Eventually, based on the attenuation coefficient of coaxial cable, the attenuation coefficient of coaxial attenuator, the directional coefficient and the effective area of horn antenna radiation port, the total power P_s of dual-frequency microwave radiated by the device can be obtained from expressions (3) and expressions (4), which is $507 \pm 11.9\%$ MW. Therefore, the efficiency of microwave power conversion is $\sim 8.8\%$. Let A_1 and A_2 be the amplitude of the two frequency components in the dual-frequency spectrum, then $|A_1|^2/|A_2|^2$ is the power ratio of the two frequency components. Furthermore, the amplitude of dual-frequency in the spectrum (Fig. 6) is roughly the same, so the power of dual frequency can be regarded as the same, about 250 MW.

IV. CONCLUSION
In this paper, a dual-frequency CRBWO is designed and studied experimentally. Using CHIPIC simulations, we have demonstrated operation of a dual-band relativistic BWO consisting of two SWSs with sinusoidal corrugations. The X-band dual-frequency spectrum obtained by experiments is 9.845 GHz and 10.517 GHz, respectively. This work provides an efficient and relatively simple structure for the dual-frequency coaxial relativistic backward wave oscillator, and experimentally measures microwave parameters including frequency, operation modes and power, which is close to the theoretical prediction and numerical simulation results.

REFERENCES
[1] V. Gaponov-Grekhov and V. L. Granatstein, *Applications of High-Power Microwaves*. Norwood, MA, USA: Artech House, 1994.
[2] C. Chen, G. Liu, W. Huang, Z. Song, J. Fan, and H. Wang, "A repetitive X-band relativistic backward-wave oscillator," *IEEE Trans. Plasma Sci.*, vol. 30, no. 3, pp. 1108–1111, Jun. 2002, doi: 10.1109/TPS.2002.801656.

[3] H. Li, "Particle simulation of tri-frequency relativistic backward-wave oscillator with resonant reflector," in *Proc. 10th Int. Vacuum Electron Sources Conf.*, 2014, pp. 1–2, doi: 10.1109/IVESC.2014.6892022.

[4] G. X. Shu, H. Yin, L. Zhang, J. P. Zhao, G. Liu, and A. D. R. Phelps, "Demonstration of a planar W-band, kW-level extended interaction oscillator based on a pseudospark-sourced sheet electron beam," *IEEE Electron Device Lett.*, vol. 39, no. 3, pp. 432–435, Mar. 2018, doi: 10.1109/LED.2018.2794469.

[5] Y. Cao *et al.*, "Over-sized mode-selective relativistic backward wave oscillator," *IEEE Electron Device Lett.*, vol. 40, no. 9, pp. 1530–1533, Sep. 2019, doi: 10.1109/LED.2019.2931259.

[6] Y. Teng *et al.*, "High-efficiency coaxial relativistic backward wave oscillator," *Rev. Sci. Instrum.*, vol. 82, no. 2, 2011, Art. no. 024701, doi: 10.1063/1.3536837.

[7] N. S. Ginzburg, R. M. Rozental, and A. S. Sergeev, "Dual band operation of the relativistic BWO," in *Proc. 4th IEEE Int. Conf. Vacuum Electron.*, 2003, pp. 181–182, doi: 10.1109/IVEC.2003.1286225.

[8] T. Wang, B.-L. Qian, J.-D. Zhang, X.-P. Zhang, C. Yi-Bing, and Q. Zhang, "Preliminary experimental investigation of a dual-band relativistic backward wave oscillator with dual beams," *Phys. Plasmas*, vol. 18, no. 1, 2011, Art. no. 013107, doi: 10.1063/1.3537818.

[9] T. Wang, J.-D. Zhang, B.-L. Qian, and X.-P. Zhang, "Dual-band relativistic backward wave oscillators based on a single beam and dual beams," *Phys. Plasmas*, vol. 17, no. 4, 2010, Art. no. 043107, doi: 10.1063/1.3368864.

[10] A. M. Elfrgani, S. Prasad, M. I. Fuks, and E. Schamiloglu, "Relativistic BWO with linearly polarized Gaussian radiation pattern," *IEEE Trans. Plasma Sci.*, vol. 42, no. 8, pp. 2135–2140, Aug. 2014, doi: 10.1109/TPS.2014.2331345.

[11] M. Elfrgani, S. Prasad, M. I. Fuks, and E. Schamiloglu, "Dual-band operation of relativistic BWO with linearly polarized Gaussian output," *IEEE Trans. Plasma Sci.*, vol. 42, no. 8, pp. 2141–2145, Aug. 2014, doi: 10.1109/TPS.2014.2331334.

[12] I. Klimov, I. K. Kurkan, S. D. Polevin, V. V. Rostov, and E. M. Tot'meninov, "A multigigawatt X-band relativistic backward wave oscillator with a modulating resonant reflector," *Tech. Phys. Lett.*, vol. 34, no. 3, pp. 235–237, Mar. 2008, doi: 10.1134/S1063785008030176.

[13] N. S. Ginzburg, R. M. Rozental, and A. S. Sergeev, "On the synthesis of radiation spectrum in a sectioned relativistic backward wave tube," *Tech. Phys. Lett.*, vol. 29, no. 2, pp. 164–167, Feb. 2003, doi: 10.1134/1.1558757.

[14] D. Chen, F. Meng, D. Wang, and Z. Fan, "Design and particle simulation of L-band bifrequency magnetically insulated transmission line oscillator," *High Power Laser Particle Beams*, vol. 21, no. 2, pp. 429–433, 2009.

[15] Y. Tang, M. Lin, H. Li, L. Zheng, B. Wang, and Y. Yin, "An X-band dual-frequency coaxial relativistic backward-wave oscillator," *IEEE Trans. Plasma Sci.*, vol. 40, no. 12, pp. 3552–3559, Dec. 2012, doi: 10.1109/TPS.2012.2222671.

[16] Y. Tang, M. Lin, H. Li, L. Zheng, B. Wang, and F. Zhang, "Design of a high-efficiency dual-band coaxial relativistic backward wave oscillator with variable coupling impedance and phase velocity," *Laser Particle Beams*, vol. 31, no. 1, pp. 55–62, Mar. 2013, doi: 10.1017/S0263034612000882.

[17] J. Liu, Y. Zhang, G. Chen, and Q. Tan, "An experimental research of using heterodyne technique for measuring frequencies of single microwave pulse," *High Power Laser Particle Beams*, vol. 9, no. 4, pp. 631–635, 1997.